IJBBE International Journal of Biophotonics & Biomedical Engineering Vol. 4, No. 1, Spring-Summer, 2024

Research Article

Modeling Skin Tissue Scattering using the Henyey-Greenstein Method: A Study of Skin Conditions

M. Ranjbaran [a,*], Sh. Zokab [a], and Z. Farsi [a]

[a] *Department of Physics, Central Tehran Branch, Islamic Azad University, Tehran, Iran*

***Corresponding Author Email: ma.ranjbaran@iau.ac.ir**

DOI: 10.71498/ijbbe.2024.1190503

ABSTRACT

Received: Nov. 14, 2024, Revised: Dec. 26, 2024, Accepted: Dec. 29, 2024, Available Online: Jan. 29, 2025

Spectral reflectance from layered skin tissue as a function of wavelength can provide valuable information about the skin's optical properties for diagnosing skin conditions. Monte Carlo and Henyey-Greenstein (HG) are two methods to model scattering in skin layers. However, the HG method is a simpler and widely used technique that assumes a single parameter to characterize the scattering phase function. In this study, we conducted simulations of scattering in six-layered skin tissue using Zemax software based on the HG method. Our observations revealed increased penetration depth and back-scattered reflectance as the wavelength increased. We investigated reflectance patterns in different skin conditions by simulating mild solar damage, mild chronic dermatitis, and Mild solar damage with chronic inflammation. We recorded differences in the maximum intensity of reflected light in each condition. Additionally, we compared the backscattered reflections produced by incoherent and coherent light sources. The results of our HD simulation-based studies suggest that incoherent sources at infrared wavelengths could be advantageous for the analysis of skin disorders.

KEYWORD

Back-scattering, Henyey-Greenstein, Skin conditions, Spectral reflectance, Zemax software.

I. INTRODUCTION

Spectral reflectance analysis holds significant potential for diagnosing skin disorders, including melanoma detection, skin cancer diagnosis, and monitoring treatment response. When light interacts with skin tissue, it is both absorbed by chromophores like melanin and hemoglobin and scattered by cells and tissue [1]. This complex interplay between absorption and scattering is key to understanding skin properties. The skin's upper layers have a complex structure with unevenly distributed components like blood vessels and pigments. This makes it difficult to accurately measure the amount of these components using light, as the reflected light signal is a mixture of contributions from different components. Despite this challenge, reflectance spectroscopy is the most common method for analyzing the skin with light [2].

Two methods are used for the optical modeling of spectral reflectance from biological tissues:

the Monte Carlo method and the Henyey–Greenstein (HG) phase function. The Monte Carlo method simulates the individual paths of photons as they travel through the tissue. It tracks each photon's interactions with the tissue, including absorption, scattering, and reflection [3, 4]. This method is highly accurate but computationally expensive, especially for complex tissue structures. However, the Henyey–Greenstein (HG) Phase Function method treats the tissue as a whole scattering body, simplifying the modeling process. It uses an analytical formula (the HG phase function) to describe the overall scattering properties of the tissue, instead of tracking each photon individually [5, 6]. This approach is much faster but sacrifices some accuracy.

C. Ash and colleagues employed Monte Carlo modeling and found that penetration depth increases with wavelength, but larger spot sizes do not significantly increase penetration beyond a certain point, highlighting the importance of understanding light-tissue interactions for optimizing therapeutic techniques [7]. O. Kim and team utilized a stochastic photon transport model and reflectance spectroscopy to study normal and bruised skin. By simulating and comparing reflectance spectra, the model accurately predicts skin changes during bruise development, including peak concentrations of bilirubin and blood volume fraction [8]. H. Funamizu and collaborators used ray-tracing software and a GPU-based Monte Carlo method to simulate light propagation in human skin, capturing its complex structure [9]. Another study demonstrated that utilizing the stable HG phase function can significantly accelerate the calculation speed of light propagation through highly scattering materials by leveraging existing a priori knowledge on interaction processes [10]. Melnikova and colleagues applied the HG phase function to estimate the reflection function of a semi-infinite and conservative scattered layer, suitable for both direct and inverse problems in atmospheric optics assuming a plane atmosphere [11]. Also, error analysis using the HG phase function through multiple scattering was carried out by Zhao and colleagues [12].

This paper presents a novel approach to modeling spectral reflectance in skin tissue, leveraging the Henyey-Greenstein (HG) phase function. This function provides a robust approximation of light scattering in biological tissues, describing the probability of light deflection after each scattering event [5]. By focusing on the HG phase function, we aim to accurately quantify the wavelength-dependent scattering of spectral reflectance. To achieve this, we have developed a comprehensive simulation using Zemax software's Non-Sequential (NSC) data editor. Our model incorporated six distinct layers representative of skin tissue. By varying the wavelength of incident light, we have simulated its penetration depth and calculated the resulting reflectance using a rectangular detector.

Also, the skin properties of mild solar damage, mild chronic dermatitis, and mild solar damage with chronic inflammation were simulated, and maximum scattering intensity was obtained. Furthermore, the simulations were compared using incoherent and coherent light sources. This detailed analysis provides a thorough understanding of how light interacts with skin at different light wavelengths, and different skin tissue conditions, ultimately informing the development of more precise and effective diagnostic tools.

II. Materials and Methods

The HG model offers a powerful tool for understanding light scattering in turbid media like biological tissues. This model utilizes a function that can predict various scattering patterns, ranging from backscattering to forward scattering, by adjusting one parameter, the anisotropy factor g, within the range $-1 \leq g \leq 1$. The angular distribution of scattered light is mathematically described as [5, 13]:

$$(\theta) = \frac{1}{4\pi} \frac{1 - g^2}{[1 + g^2 - 2g\cos(\theta)]^{3/2}} \quad (1)$$

Where $p(\theta)$ represents a probability density function and θ ranges from 0 to π radians,

indicating the angle between the photon's pre- and post-scattering directions. A value of θ = 0 rad denotes that the photon continues in its original direction post-collision.

TABLE 1. LENS DATA EDITOR OF SIMULATION

	Object Type	Comment	Ref Object	Z Position		Z Length	Material (refractive index)	X Half Width
1	Source File	AVAG-QSM-01-	0	-1.000		0.100	1.34	100
2	Rectangular Volume	Epidermis	1	0.000		0.100	1.4	10.000
3	Rectangular Volume	Papillary dermis	2	0.100	p	0.150	1.39	10.000
4	Rectangular Volume	Upper blood net dermis	3	0.150	P	0.100	1.4	10.000
5	Rectangular Volume	Reticular dermis	4	0.100	P	1.500	1.39	10.000
6	Rectangular Volume	Deep blood net dermis	5	1.500	P	0.100	1.44	10.000
7	Rectangular Volume	Subcutaneous fat	6	0.100	p	6.000	1.34	10.000
8	Detector	Small sensor	0	-0.200		100	ABSORB	5.000

TABLE 2. OPTICAL PROPERTIES OF HUMAN SKIN [4].

Wavelength(nm)	Skin layer	Thickness(mm)	g	n	$\mu_a(cm^{-1})$	$\mu_s(cm^{-1})$
600	Epidermis	0.1	0.85	1.34	0.015	40
	Papillary dermis	0.1	0.8	1.4	0.07	30
	Upper blood net dermis	0.15	0.9	1.39	0.1	35
	Reticular dermis	0.1	0.76	1.4	0.07	20
	Deep blood net dermis	0.1	0.95	1.39	0.1	35
	Subcutaneous fat	6	0.8	1.44	0.03	15

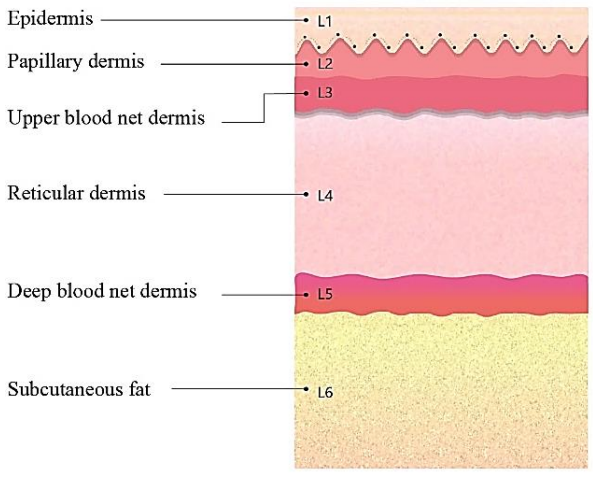

Fig. **1**. The model of six-layered skin tissue.

An isotropic medium is characterized by g = 0, indicating an equal likelihood for the photon to travel in any direction. Therefore, the outcome is influenced by the anisotropy factor g, which is denoted as $g=\langle\cos(\theta)\rangle$ [14].

In the context of human skin, the HG model represents the skin as six distinct layers: the epidermis, papillary dermis, upper blood net dermis, reticular dermis, deep blood net dermis, and subcutaneous fat. These layers are modeled as rectangular volumes with no distance between them, effectively treating each layer as a continuation of the previous one (as shown in Fig. 1).

To simulate light scattering within the skin, the refractive index, thickness, and position of each skin layer as listed in Table 1, were inputted into the Lens data editor of Zemax software. Initial parameters within the "bulk scatter" module were then adjusted to model wavelength-dependent scattering. These parameters include: g, Mean path, and Transmission fraction. The mean path and transmission coefficients were calculated using the following equations [3]:

$$Mean\ path = \frac{1}{\mu_a + \mu_s} \quad (2)$$

$$Transmission = \frac{\mu_s}{\mu_a + \mu_s} \quad (3)$$

Where the absorption coefficient (μ_a) and scattering coefficient (μ_s) are fundamental parameters in light propagation through biological tissues. μ_a quantifies the absorption of light energy by the tissue, representing the conversion of photons into other forms of energy within the cells. Conversely, μ_s describes the scattering of light, characterized by the change in the direction of photons as they interact with tissue components. Table 2 presents the specific values of these coefficients used in a 6-layer skin model for a wavelength of 600 nm [15].

To determine the spectral reflectance, a rectangular detector with a 180° field of view, 5 mm in length, and 10^4 pixels was positioned 0.1 mm along the skin surface.

The modeling was performed in the non-sequential data editor of the Zemax simulation software. In the bulk scatter section of each layer's properties, based on Henyey-Greenstein-bulk.DLL, mean path and transmission values can be calculated based on substituting μ_a and μ_s in equations 2 and 3. By applying the coefficients g and n for each layer, representing the anisotropy factor and refractive index respectively, scattering within the skin layers for each wavelength can be observed by referring to ray tracing in the analysis section.

The coefficients g and n are dependent on the input wavelength. Simulations were conducted for wavelengths of 337, 442, 575, 600, 633, and 940 nm [15, 16]. The resulting spectral diagram illustrates the scattering intensity at each wavelength.

In every skin condition, changes in the thickness of skin layers lead to alterations in the structure of skin tissues, which are manifested in the scattering coefficients. To simulate the skin conditions, the thickness of each skin layer is altered in response to conditions like mild solar damage, mild chronic dermatitis, and mild solar damage with chronic inflammation [17]. Then the maximum back-scattering intensity was compared with normal skin.

III. Results and Discussions

The angular distribution of HG-based scattered rays in the multilayered skin tissue is presented in Fig. 2. The NSC 3D layout shows the layered skin tissue including living epidermis, papillary dermis, upper blood net dermis, reticular dermis, deep blood net dermis, and subcutaneous fat.

The irradiation may undergo repeated scattering events within the skin tissue, with the scattered rays potentially traversing multiple times through the medium before being absorbed or emerging on the other side. As can be seen, the reflectance is obviously dependent on the wavelength of the irradiation source. The 337 nm irradiation reaches the epidermis skin layer, while the 633 nm irradiation penetrates the deeper layers, skin subcutaneous tissue [18].

To detect the back-scattered reflection, we incorporated a rectangular detector into the simulation. The detector was positioned at a small distance, 0.1 mm, from the skin's surface. The profile and intensity of back-scattered rays for incoherent irradiance at 337 nm, and 940 nm can be seen in Fig. 3. The concentrated light with higher intensity was detected at higher wavelength.

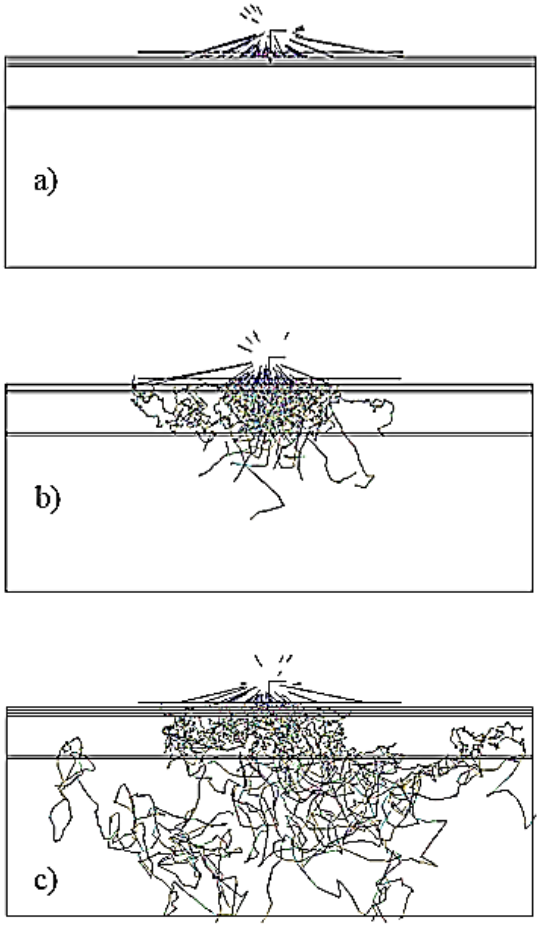

Fig. **2**. 3D layout of multilayered skin tissue at wavelength of a) 337 nm, b) 575 nm, and c) 633 nm.

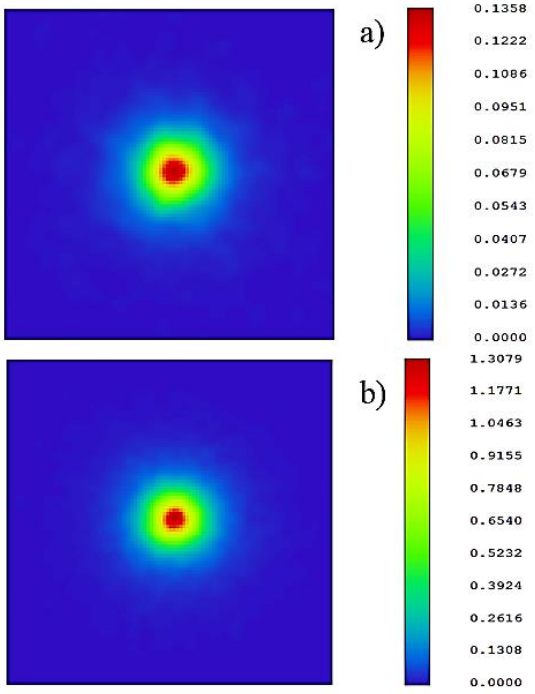

Fig. **3**. Detector view at wavelengths of a) 337 nm, and b) 940 nm.

To obtain the spectral reflectance from multilayered skin tissue, the incoherent irradiation sources at various wavelengths, λ, 337, 442, 575, 600, 633, and 940 nm were considered. We input the specific optical properties of each skin layer, $\mu_a(\lambda)$, $\mu_s(\lambda)$, g(λ), and n(λ), corresponding to each wavelength, into the Zemax software for simulation. The cross-section row of the detector viewer at each wavelength is depicted in Fig.4. It is obvious that the reflectance increased with increasing wavelength.

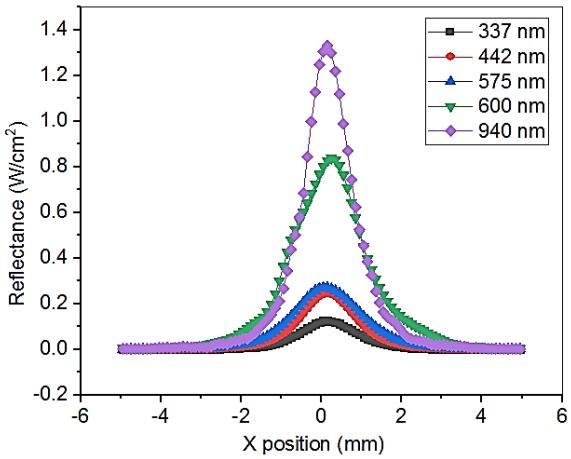

Fig. **4**. The back-scattered light profile at different wavelengths.

Fig.5 shows the peak intensity of the reflected light in the wavelength range of 337 to 940 nm. This figure shows an increase of around 600 nm due to more scattering by skin structures [3, 18]. While, at shorter wavelengths, light is more likely to be absorbed by melanin, Hemoglobin, and other chromophores in the skin, leading to reduced reflectance [20, 21]. This trend is significant because the interaction of light with these chromophores can provide insights into the skin's physiological conditions and overall health.

TABLE. 3. VARIATION OF SKIN LAYERS THICKNESS IN DIFFERENT SKIN CONDITIONS AND ASSOCIATED BACK-SCATTERING INTENSITY.

Skin conditions	Thickness(mm)					Max back-scattering intensity
	Epidermis	Papillary dermis	blood net dermis	Reticular dermis	Deep blood net dermis	
Normal skin	0.1	0.15	0.1	1.5	0.1	1.56
Mild solar damage	0.03	0.016	0.01	0.162	0.01	1.35
Mild chronic dermatitis	0.09	0.024	0.016	0.240	0.016	1.47
Mild solar damage, chronic inflammation	0.05	0.016	0.01	0.162	0.01	1.40

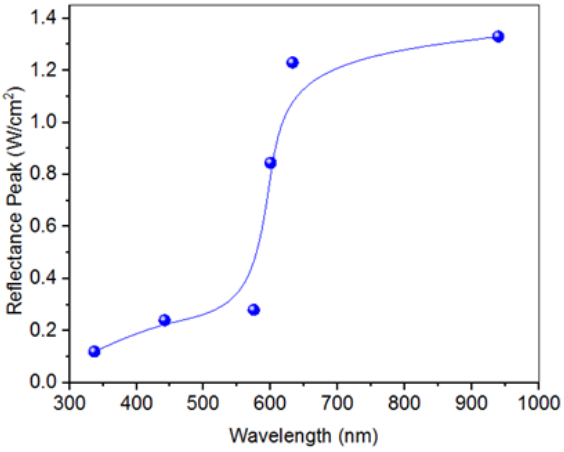

Fig. **5**. Reflectance peak as a function of wavelength.

As the penetration depth and the reflectance in the near IR regime (940 nm) were more, it was selected for more analysis. To analyze the reflectance in different skin conditions, in accordance with Table 3, the mild solar damage, mild chronic dermatitis, and mild solar damage with chronic inflammation were simulated and the maximum intensity of reflection was recorded. As can be seen, the thinner the layers become, the less reflection occurs [22]. Understanding these variations is crucial for developing non-invasive diagnostic tools that employ optical methods for skin analysis. Additionally, external factors such as illumination conditions, can also influence the peak intensity of reflected light. In Fig. 6, a comparison was made between the back-scattered reflections produced by incoherent irradiance (e.g., LED) and coherent irradiance (e.g., laser) at 940 nm. It is evident that while the peak intensity of back-scattered light is lower when using incoherent irradiance, it tends to be more isotropic, meaning the light is scattered uniformly in various directions.

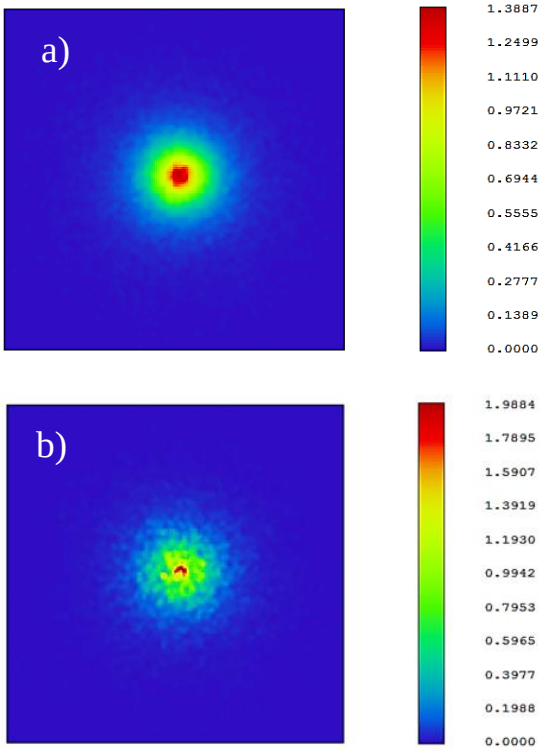

Fig. **6**. Detector view at wavelengths of 940 nm using a) incoherent irradiance, and b) coherent irradiance.

The backscattered laser light exhibited speckle patterns (fluctuations in intensity) due to the coherent nature of laser light. Variations in path length, resulting from multiple scattering and differing refractive indices within tissue layers, introduced phase shifts to the light waves. This phenomenon caused constructive and destructive interference between multiple scattered light waves, creating bright and dark spots [23, 24]. Furthermore, minor cellular movements or refractive index changes alter the interference pattern, causing observable speckle pattern fluctuations [25]. The speckles pattern could be utilized in the Laser speckle contrast imaging technique to monitor the dynamics of skin tissue [26].

Also, Fig. 7 illustrates a comparison of the cross-sectional row of backscattered reflections obtained using both incoherent (LED) and coherent (laser diode) illumination. This comparison reveals that employing a laser diode as the light source resulted in higher sensitivity compared to using an LED [27]. However, the laser diode illumination resulted in a non-uniform cross-sectional profile. Therefore, LEDs could be advantageous in the diagnosis and treatment of skin conditions [28].

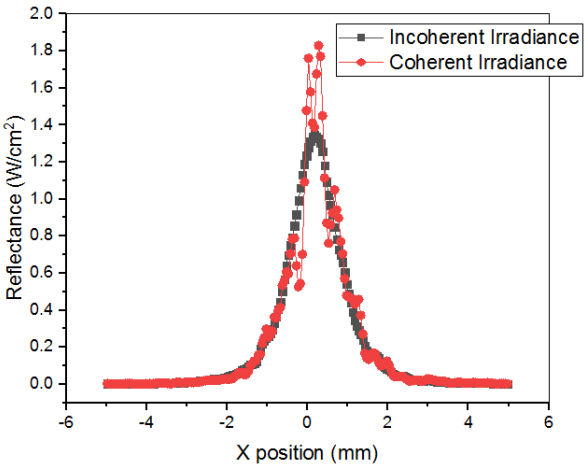

Fig. **7**. Cross section row of back-scattered reflection using incoherent irradiance, and coherent irradiance.

IV. Conclusion

Simulation allows researchers to study the optical properties of skin tissue in different conditions. Monte Carlo and Henyey-Greenstein methods are two alternative approaches to model scattering in skin layers. However, HG is a good alternative when complexity is not necessary. In this paper, based on the simulation of the skin layer's parameters in the HG method, the back-scattered reflectance was obtained at different wavelengths. Our results highlight the potential for using longer wavelengths to enhance light delivery and detection in the skin.

Also, different skin conditions such as mild solar damage, mild chronic dermatitis, and mild solar damage with chronic inflammation were simulated and the back-scattered reflectance intensity was recorded at the detector. The findings demonstrated that decreasing layer thickness led to a reduction in reflected light. Furthermore, when comparing coherent and incoherent light sources, we observed that coherent light resulted in a more intense reflection, but this reflection was distributed non-uniformly. Our results suggest that the HG method can be a valuable tool for optimizing light-based applications such as dermatological imaging, skin diagnostics, and phototherapy.

References

[1] N. Kollias, G. Zonios, and G. N. Stamatas, "Fluorescence spectroscopy of skin. Vibrational Spectroscopy," Vol. 28, pp. 17-23, 2002.

[2] I. V. Meglinskii, "Monte Carlo simulation of reflection spectra of random multilayer media strongly scattering and absorbing light," Quantum Electronics, Vol. 31, pp. 1101, 2001.

[3] I. T. Maeda and N. Arakawa, M. Takahashi, & Y. Aizu, "Monte Carlo simulation of spectral reflectance using a multilayered skin tissue model," Optical review, Vol. 17, pp. 223-229. 2010.

[4] I. V. Meglinski and S. J. Matcher, "Computer simulation of the skin reflectance

spectra,"Computer methods and programs in biomedicine, Vol. 70, pp. 179-186, 2003.

[5] T. Binzoni, T. S. Leung, A. H. Gandjbakhche, D. Ruefenacht, and D. T. Delpy, "The use of the Henyey–Greenstein phase function in Monte Carlo simulations in biomedical optics," Physics in Medicine & Biology, Vol. 51, pp. N313, 2006.

[6] L. G. Henyey and J. L. Greenstein, "Diffuse radiation in the galaxy. Astrophysical Journal," Vol. 93, pp. 70-83, 1941.

[7] C. Ash, M. Dubec, K. Donne, & T. Bashford, "Effect of wavelength and beam width on penetration in light-tissue interaction using computational methods," Lasers in medical science, Vol. 32, pp. 1909-1918, 2017.

[8] O. Kim, J. McMurdy, C. Lines, S. Duffy, G. Crawford, and M. Alber, "Reflectance spectrometry of normal and bruised human skins: experiments and modeling. Physiological measurement," Vol. 33, pp. 159-175, 2012.

[9] H. Funamizu, T. Maeda, S. Sasaki, I. Nishidate and Y. Aizu, "Simulation of spectral reflectances in human skin tissue using ray tracing and GPU-based Monte Carlo method," Optical Review, Vol. 21, pp. 359-363, 2014.

[10] V. M. Petnikova, E. V. Tret'yakov and V. V. Shuvalov, "Stability of the Henyey—Greenstein phase function and fast path integration under conditions of multiple light scattering," Quantum Electronics, Vol. 36, pp. 1039, 2006.

[11] I. N. Melnikova, Z. M. Dlugach, T. Nakajima, K. Kawamoto, "Calculation of the reflection function of an optically thick scattering layer for a Henyey–Greenstein phase function". Applied optics, Vol. 39(24), pp. 4195-4204. 2000.

[12] Zhao, G., & Sun, X. "Error analysis of using henyey-greensterin in Monte Carlo radiative transfer simulations," In Progress in Electromagnetics Research Symposium, pp. 1424-1427, 2010.

[13] Petnikova, V. M., Shuvalov, V. V., & Tret'akov, E. V. "Multiple-scattering Henyey-Greenstein phase function and fast path-integration," ICONO 2007: Nonlinear Laser Spectroscopy and High-Precision Measurements; and Fundamentals of Laser Chemistry and Biophotonics, SPIE. Vol. 6727, pp. 311-316, 2007.

[14] N. S. Żołek, S. Wojtkiewicz and A. Liebert, "Correction of anisotropy coefficient in original Henyey Greenstein phase function for Monte Carlo simulations of light transport in tissue," Biocybernetics and Biomedical Engineering, Vol. 28, pp. 59-73, 2008.

[15] A. P. Popov, A. V. Priezzhev, and R. Myllyla, "Effect of spectral width on short laser pulse propagation through upper layers of human skin: Monte Carlo simulations," Proc. SPIE 5319, Laser Interaction with Tissue and Cells XV, (1 July 2004).

[16] V. Tuchin, "Tissue Optics: Light Scattering Methods and Instruments for Medical Diagnosis," SPIE Press, Washington, 2000.

[17] T. L. Troy and S. N. Thennadil, "Optical properties of human skin in the near infrared wavelength range of 1000 to 2200 nm," Journal of biomedical optics, Vol. 6, pp. 167-176, 2001.

[18] M. D. Francisco, W. F. Chen, C. T. Pan, M. C. Lin, Z. H. Wen, C. F. Liao, & Y. L. Shiue, "Competitive real-time near infrared (NIR) vein finder imaging device to improve peripheral subcutaneous vein selection in venipuncture for clinical laboratory testing. Micromachines," Vol. 12, pp. 373-1-21, 2021.

[19] G. Zonios and A. Dimou, "Light scattering spectroscopy of human skin in vivo," Optics Express, 17, 1256-1267, 2009.

[20] S. H. Tseng, P. Bargo, A. Durkin, and N. Kollias, "Chromophore concentrations, absorption and scattering properties of human skin in-vivo," Optics express, Vol. 17, pp. 14599-14617, 2009.

[21] V. Mircheva, E. Borisova, T. Genova, P. Troyanova, L. Avramov and A. Markovski, "Diagnosis of skin lesions through prototype clinical device with diffuse reflectance spectroscopy," Journal of Physics: Conference Series, Vol. 2487, pp. 012026 (1-5), 2023.

[22] P. Hanrahan and W. Krueger, "Reflection from layered surfaces due to subsurface scattering," In Seminal Graphics Papers: Pushing the Boundaries, Vol. 2, pp. 279-288, 2023.

[23] G. R. Ge, J. P. Rolland and K. J. Parker, "Speckle statistics of biological tissues in

optical coherence tomography," Biomedical Optics Express, Vol. 12, pp. 4179-4191, 2021.

[24] Y. Zhang, C. Wang, S. Tong and P. Miao, "Separating single-and multiple-scattering components in laser speckle contrast imaging of tissue blood flow," Biomedical Optics Express, Vol. 13, pp. 2881-2895, 2022.

[25] N. N. Boustany, S. A. Boppart, and V. Backman, "Microscopic imaging and spectroscopy with scattered light," Annual review of biomedical engineering, Vol. 12, pp. 285-314, 2010.

[26] S. Zheng and J. Mertz, "Direct characterization of tissue dynamics with laser speckle contrast imaging," Biomedical Optics Express, Vol. 13, pp. 4118-4133, 2022.

[27] N. S. Hanasil, R. K. R. Ibrahim, F. H. Mustafa, F. K. C. Harun, and A. A. Tan, "Evaluation of NIR LED and laser diode as a light source in diffuse reflectance spectroscopy system for intravenous fluid infiltration detection under dermis layer of skin phantom," Measurement, Vol. 223, pp. 113707-1-6, 2023.

[28] M. A. Dall Agnol, R. A. Nicolau, C. J. de Lima, and E. Munin, "Comparative analysis of coherent light action (laser) versus non-coherent light (light-emitting diode) for tissue repair in diabetic rats," Lasers in medical science, Vol. 24, pp. 909-916, 2009.

THIS PAGE IS INTENTIONALLY LEFT BLANK.